This article has been accepted for publication in a future issue of this journal, but has not been fully edited. Content may change prior to final publication. Citation information: DOI 10.1109/TSM.2018.2865167, IEEE Transactions on Semiconductor Manufacturing

Nanoscale metrology of line patterns on semiconductor by continuous wave terahertz multispectral reconstructive 3D imaging overcoming the Abbe diffraction limit

Anis Rahman, *CTO,* and Aunik K. Rahman, Sr. Engr., *Applied Research & Photonics, Inc.*

***Abstract*— This paper demonstrates overcoming of the Abbe diffraction limit (ADL) on image resolution. Here, terahertz multispectral reconstructive imaging has been described and used for analyzing nanometer size metal lines fabricated on a silicon wafer. It has also been demonstrated that while overcoming the ADL is a required condition, it is not sufficient to achieve sub-nanometer image resolution with longer wavelengths. A nanoscanning technology has been developed that exploits the modified Beer-Lambert's law for creating a measured reflectance data matrix and utilizes the 'inverse distance to power equation' algorithm for achieving 3D, sub-nanometer image resolution. The nano-lines images reported herein, were compared to SEM images. The terahertz images of 70 nm lines agreed well with the TEM images. The 14 nm lines by SEM were determined to be ~15 nm. Thus, the wavelength dependent Abbe diffraction limit on image resolution has been overcome. Layer-by-layer analysis has been demonstrated where 3D images are analyzed on any of the three orthogonal planes. Images of grains on the metal lines have also been analyzed. Unlike electron microscopes, where the samples must be in the vacuum chamber and must be thin enough for electron beam transparency, terahertz imaging is non-destructive, non-contact technique without laborious sample preparation.**

***Index Terms*—Metrology; Imaging; Volume measurement; Nanotechnology; Nondestructive testing.**

I. Introduction

Nanometer metal lines are the key for on chip interconnects where the feature sizes are approaching 10 nm and below. While fabrication of metal lines with 10 nm dimensions have been demonstrated, there is no obvious way for accurately measure their dimensions non-invasively. Current characterization techniques, such as scanning electron microscope (SEM), transmission electron microscope (TEM), atomic force microscope (AFM), scanning tunneling microscope (STM), and focused ion beam (FIB) have been established and practiced over the past decades. While these techniques are effective and accurate, they are destructive, require tedious and time-consuming sample preparation. Additionally, the above-mentioned techniques produce a frozen-in-time image of a single surface. A semiconductor wafer, for example, must be cut for inspection across its thickness. Samples may be only as big as it may fit in the sample chamber that must be kept under high vacuum. Up until now, there has not been an alternative to characterizing a whole wafer, both on its surface and across the thickness, or the sub-surface, in a non-destructive, non-contact mode, with layer by layer inspection capability. Inevitably, semiconductor manufacturing is a complicated process where a wafer must undergo a number of critical tests, both in the blank form, at various stages of process development, and at the final stage with patterned devices. It is a laborious but unavoidable task to conduct testing at multiple stages for successful chip manufacturing. Especially, when the feature sizes are being reduced to 10 nm and below, the cost for multi-stage testing increases exponentially, which can significantly impact the cost of advanced technology products. Thus, the cost benefit to the end users that is expected from miniaturization of several orders of magnitude, is far from realization.

To this end, it appears that the scientific and the technical community is being held hostage to the fact that physics dictates that the ultimate image resolution is set by the wavelength of the light used for imaging, the Abbe diffraction limit ("ADL"). Ernst Abbe in 1873 [1] found that light with wavelength λ, traveling in a medium with refractive index n and converging to a spot with half-angle θ will make a spot with radius, $d = \frac{\lambda}{2n\sin\theta}$, where, $n\sin\theta$ is called the numerical aperture (NA). Approximating $NA = 1$ (i.e., for vacuum), the lowest spot size (resolution) is $\lambda/2$. Since the wavelength of electrons is much smaller than that of photons (2.5 pm at 200 keV), the resolution of an electron microscope is theoretically unlimited. Practically, the resolution of an electron microscope is limited to ~0.1 nm due to its objective lens system.

Beating the diffraction limit has become one of the primary goal of research in modern optics [2], so, a question arises, "is the Abbe diffraction limit unavoidable?" The objective of the present work is to demonstrate one approach where the image formation mechanism is independent of the wavelength of the radiation used and thus, the Abbe diffraction limit has been

This paper is based in parts on a presentation made at the ASMC 2017, Saratoga Springs, NY. The authors are with Applied Research & Photonics, Inc., 470 Friendship Road, Suite 10, Harrisburg, PA 17111, USA (email: a.rahman@arohotonics.net).

0894-6507 (c) 2018 IEEE. Personal use is permitted, but republication/redistribution requires IEEE permission. See http://www.ieee.org/publications_standards/publications/rights/index.html for more information.

This article has been accepted for publication in a future issue of this journal, but has not been fully edited. Content may change prior to final publication. Citation information: DOI 10.1109/TSM.2018.2865167, IEEE Transactions on Semiconductor Manufacturing

avoided. We have recently reported on the multispectral reconstructive imaging of quantum dots [3], epitaxial semiconductor layers [4] as well as on soft tissues [5] where the dimension of the imaged objects are smaller than the wavelength of terahertz radiation (T-ray). The nanometer and sub-nanometer image resolution obtained by reconstructive technique was validated by corresponding TEM images (except for the soft tissues where TEM images were not available); they were found in good agreement within the experimental error limits. As we will demonstrate below for the case of metal lines on silicon wafer, the technique reported herein does produce results in good agreement with SEM images as well. Therefore, it may be claimed that the terahertz multispectral reconstructive imaging technique reported in this paper is indeed capable of breaking the wavelength barrier as imposed by the Abbe diffraction limit. However, as will also be shown below, while overcoming the ADL is a required condition for achieving higher image resolution, it is not sufficient for achieving sub-nanometer image resolution. Hence, a stratagem has also been devised for achieving sub-nanometer image resolution.

In what follows, we first review the principle of reconstructive imaging (RI) adapted in this work. Then we describe a stratagem for overcoming the ADL and achieving sub-nanometer image resolution. Afterwards, we present and analyze images of nanometer size metal lines and compare them with corresponding SEM images followed by some concluding remarks.

II. MULTISPECTRAL RECONSTRUCTIVE IMAGING

Terahertz multispectral reconstructive imaging and terahertz time-domain spectrometry for investigating different semiconductor wafers and nanomaterials has been described elsewhere [3], [4]. Reconstructive imaging offers an important opportunity to define one's own pixel size (or voxel size in 3D) by a hardware and software combination, as opposed to being limited by the image sensor chip such as the charged coupled device (CCD). A comparison of the mechanisms of a digital camera and the RI is shown in Fig. 1. As outlined (Fig. 1), a digital camera displays and records the processed signal of an object that is focused on a CCD by means of a lens. The output of the CCD is processed by a built-in processor which displays the image and saves it in a file. In contrast, the reconstructive route eliminates the focusing lens and the CCD. Instead, the object to be imaged is scanned along the 3 orthogonal axes; the reflected signal (or, equivalently, the transmitted signal) is recorded in a data file and then processed by a suitable algorithm. The procedure for 3D image formation is outlined below; first the data structure and then the image formation algorithm are described followed by the required conditions for sub-nanometer image resolution.

A. Data structure

3D imaging requires a value of a voxel, which is the smallest unit corresponding to a 3D space; i.e., $\{x, y, z, v\}$, where $\{x, y, z,\}$ are the three orthogonal coordinates and v is the value of the reflected intensity at that point. To characterize a 3D space, data need to be recorded for all of a given 3D volume. This is best done by an experimental scanning protocol where the volume is divided in to a number of slices (surfaces) and the slices are scanned one after another. Thus, the data are generated in the following sequence: for every $\{z_1, y_1\}$, a line is scanned giving $\{x_1,\ x_2 \dots\ x_n\}$. Then the line is repeated for y_2 through y_n, while keeping the z_1 (i.e., the depth) fixed.

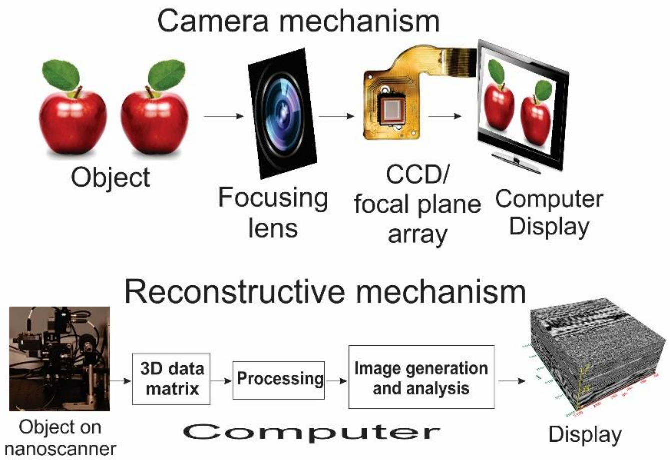

Fig. 1. Comparison of image formation scheme in a camera and in reconstructive imaging.

This sequence of line scans at a given interval thus generates data for the first slice (surface) of the volume. Then, the whole scan is repeated for z_2, yielding the second slice of the volume. This process is then repeated for all the slices along the Z-axis in order to digitize the whole volume. The line scan is done by a streaming data acquisition protocol, where, a command is issued to move the scanner from the start point to the end point along the x-axis. As the positioning stage moves, its instantaneous position and the reflected intensity at that point are recorded by the computer interface; thus, generating the $\{x_1,\ x_2 \dots\ x_n\}$ points for a given $\{z_i, y_j\}$. The reflected intensity, or both the reflected and transmitted intensity, is read simultaneously corresponding to each x_i. Once the whole volume is scanned, the data set is then used for generating the image via a suitable algorithm such as the "inverse distance to power equations," [6], [7] as described below.

B. Inverse distance to power equation

This is a method for grid-based map creation from measured $\{x, y, z, v\}$ data set. Practical $\{x, y, z\}$ based data are typically comprised of irregularly spaced values; as such it requires further computation to generate a grid-based map (or a lattice). The gridding process effectively interpolates data values for the lattice at locations where data values are absent. Therefore, the closer the measured data points are to each other, the more accurate the gridded image is for feature sizes that are smaller than the hardware resolution. The experimental setup used for the present work has a hardware resolution of ~24 nm. Therefore, the interpolation via inverse gridding method is used to generate an image at 1 nm resolution or less. The reliability of the interpolation is tested by calibration with respect to known dimensions [3]. A smoothing parameter may be applied during interpolation in order to suit the imaging requirements

0894-6507 (c) 2018 IEEE. Personal use is permitted, but republication/redistribution requires IEEE permission. See http://www.ieee.org/publications_standards/publications/rights/index.html for more information.

This article has been accepted for publication in a future issue of this journal, but has not been fully edited. Content may change prior to final publication. Citation information: DOI 10.1109/TSM.2018.2865167, IEEE Transactions on Semiconductor Manufacturing

for a given specimen. The method does not extrapolate values beyond those found in the scanned data matrix. The following equations are used for computation of the 3D lattice via inverse distance to a power [7], [8]:

$$\hat{C}_j = \frac{\sum_{i=1}^{n} \frac{C_i}{h_{ij}^{\beta}}}{\sum_{i=1}^{n} \frac{1}{h_{ij}^{\beta}}} \tag{1}$$

where, $h_{ij} = \sqrt{d_{ij}^2 + \delta^2}$,

h_{ij} is the effective separation distance between grid node "j" and the neighboring point "i;"

$\hat{C}_j$ are the interpolated values for lattice node "j;"

C_i are the neighboring measured points;

d_{ij} is the distance between grid node "j" and the neighboring point "i;"

β is the power or weighting parameter; and

δ is the smoothing parameter.

The power, β and the smoothing factor, δ, in the above computation may be chosen by the user to suit different imaging needs. Once the lattice is calculated, the surface image and volume image are generated by simply rendering the grid with a chosen color scheme. As an illustration of the functionality of the algorithm, consider a simple function, $f(x, y, z) = c * cos(x)$ to demonstrate the image formation. One can easily compute this function over a given 3D space. Let us assume the data range: $x \to 0 \ldots 3\pi, y \to 0 \ldots 6$, z and the value are calculated for a given c. Once the function is evaluated via the procedure described above, one can construct the data space. Then using the gridding method, one can reconstruct (map) the function over the given 3D space. The plot for the above function looks like as shown in Fig. 2. Closer the grid points, smoother will be the surface. One can plot experimental data by the same procedure.

C. Overcoming the Abbe diffraction limit and achieving sub-nanometer resolution

As outlined in Fig. 1, the case of image formation by a camera is totally dependent on the wavelength of the light used for imaging; as such it must obey the Abbe diffraction limit. Overcoming the ADL implies that the technique must be capable of resolving an object whose size is smaller than half the wavelength of the energizing radiation.

In case of multispectral terahertz radiation (T-ray), the wavelengths are much bigger than the visible spectrum. For example, the terahertz source of the current experimental setup has a range of 0.1 THz to ~33 THz [9]. Thus, the wavelength range is wide (multispectral); from ~9 µm up to ~3000 µm. Consequently, breaking the ADL demands that one only needs to demonstrate a resolution of less than 4.5 µm or so. Therefore, just overcoming the ADL in and of itself is not sufficient to resolve nanometer or smaller dimension objects. The real challenge is to achieve an image resolution of 1 nm or smaller

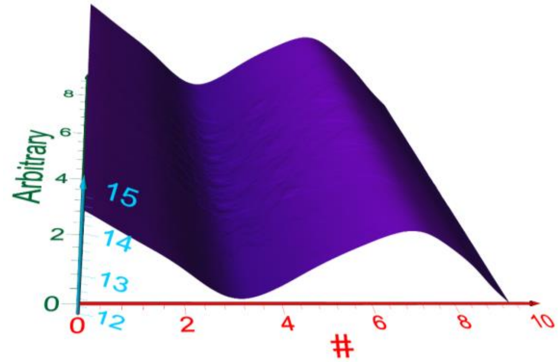

Fig. 2. A 3D plot of the function $f(x, y, z) = c * cos(x)$.

by using an energy whose wavelength is much bigger than the object to be imaged without utilizing an electron microscope. Here, a stratagem has been formulated to achieve sub-nanometer image resolution, that both overcomes the ADL and also offers an ability of a very high zooming factor for imaging objects from macro dimensions down to sub-nanometer dimensions. The main steps are described below.

For the multispectral reconstructive imaging, the wavelength (diffraction) effect is avoided by scanning an object and utilizing the reflected intensity matrix for image generation (see Fig. 1). The reconstructive imaging can be implemented, in principle, by any light source and detector system, similar to what is done in regular topography and tomography, but to be able to see under the surface in a non-destructive fashion, only terahertz is suitable via the RI mode because of its ultra-sensitivity [10]. In this case, a simple tomogram is not enough, as was shown elsewhere [11]. However, here we exploit the Beer-Lambert law, rewritten in terms of the measured reflectance as, R=αlϵ, where α is the molar absorptivity, l is the path length, and ϵ is the dielectric constant. Measured reflectance, R is a material dependent parameter, thus, also dependent on the position of the incident beam on the sample under measurement, because, the sample (e.g. a semiconductor wafer) is made of different materials arranged in different patterns. Thus, a 3D matrix of the position dependent reflectance is adequate for reconstructing an image of the volume via the algorithm outlined above.

With the advent of this nanoscanner, the resolution limit is partly defined by the smallest step of the positioning system. This is ~24 nm for the current setup. Thus, using the algorithm as described above, the resolution is enhanced down to less than 1 nm. The algorithm outlined here will only interpolate the measured data, it never extrapolates; thus, ensures that the results are within the boundaries of the object under investigation. With the combination of an even finer positioning stage and the algorithm, it is projected that the resolution may be enhanced down to a few Angstroms (Å).

III. EXPERIMENTAL

The experimental arrangement was reported elsewhere [10] and reproduced in Fig. 3. An Applied Research & Photonics terahertz nanoscanning spectrometer (TNS) was used for the present investigation. There are two main parts of the TNS, the terahertz module and the nanoscanner module. The terahertz

0894-6507 (c) 2018 IEEE. Personal use is permitted, but republication/redistribution requires IEEE permission. See http://www.ieee.org/publications_standards/publications/rights/index.html for more information.

This article has been accepted for publication in a future issue of this journal, but has not been fully edited. Content may change prior to final publication. Citation information: DOI 10.1109/TSM.2018.2865167, IEEE Transactions on Semiconductor Manufacturing

module generates multispectral continuous-wave terahertz energy via the dendrimer dipole (DDE) mechanism [9] and also generates time-domain interferogram via an optical delay-line. The terahertz beam is coupled to a multimode fiber [3] that delivers the beam to the optical circuit located on the nanoscanner module. Additionally, the nanoscanner module houses the three orthogonal axes and an optical circuit for focusing the terahertz beam on the sample as well as the detection system. Both reflection mode and transmission mode measurements are possible. Here, the sample remains stationary while the nanoscanner will scan the sample over a chosen area or volume. As pointed out before, the nanoscanner has a hardware pitch of ~24 nm in all three orthogonal directions. This is the scanning resolution used for the current measurements. The scanned data matrix was stored in a data file and processed by the aforementioned algorithm as implemented by a commercially available software.

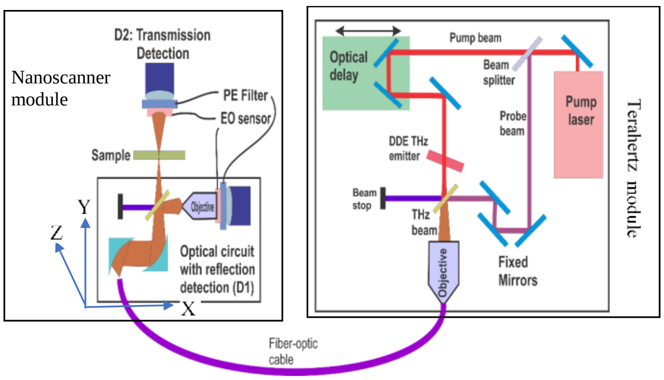

Fig. 3. The optical circuit is mounted on a XYZ nanoscanner (not shown). Both reflection mode and transmission mode measurements are possible. Here, the sample remains stationary while the nanoscanner will scan the sample over a chosen area or volume. Adapted from [10].

Two sample chips with different metal line patterns were obtained from NGR Inc. [8]. These chips have different types of metal lines on them with different dimensions; all deposited on the surface of a silicon wafer. As determined by NGR Inc. via SEM, the first group of lines are 14 nm wide and the second group of lines are 70 nm wide. These data are shown in Fig. 4 as supplied by NGR Inc. The as received chips were mounted on the TNS one at a time and scanned over a small volume. Built-in front end software interface was used for data acquisition via aforementioned scanning protocol over selected areas and volumes of the chip.

IV. RESULTS AND DISCUSSION

Experimental results are compared with the NGR Inc. data as shown in Table 1. In Fig. 4 we display three images obtained courtesy of NGR Inc. Fig 4(a) is a SEM image of 70 μm^2 area of a chip while Fig. 4(b) displays a single metal line of width 70 nm. Fig. 4 (c) shows a line pattern of width 14 nm as reported by NGR Inc.

We now present and analyze the terahertz images. Fig. 5 shows an image of 100 μm^2 area of a chip produced by terahertz multispectral reconstructive imaging. Subsequent analysis is presented for 15 nm line patterns and then 70 nm patterns, respectively.

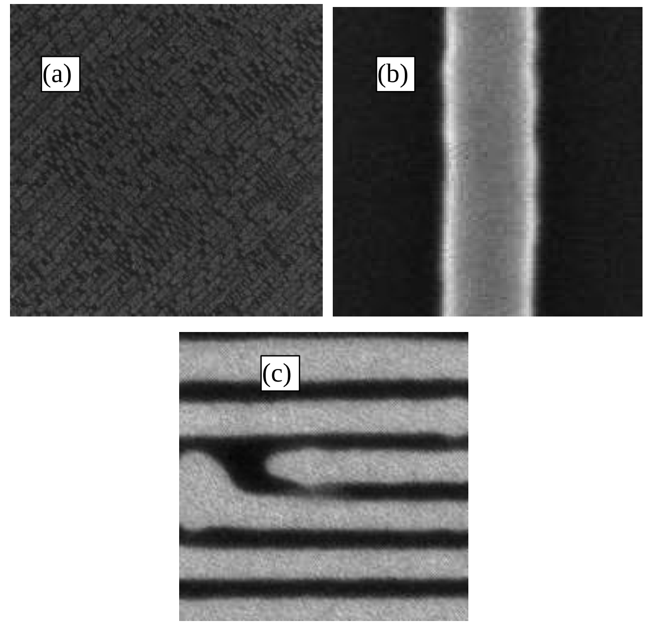

Fig. 4. Comparison with SEM images (from NGR Inc.) of (a) 70 μm x 70 μm area; (b) 70 nm line; and (c) 14 nm lines [8]. Although no scales are shown on the SEM images, the dimensions of each feature are clearly noted in the NGR Inc.'s source file.

TABLE - I
UNITS FOR MAGNETIC PROPERTIES

Feature	NGR Inc. SEM data [8]	Terahertz data
70 nm line pattern	70 nm	70 nm ± x nm
14 nm line pattern	14 nm	~15 nm ± x nm

x is the standard deviation that could be computed from multiple measurements.

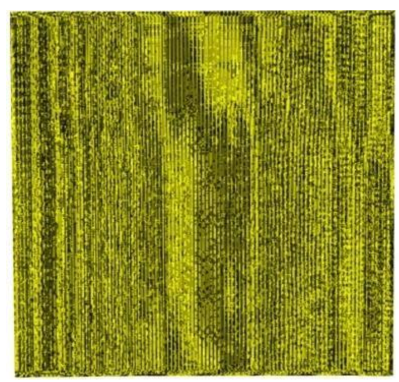

Fig. 5. Terahertz image of a 100 μm^2 area of a test chip with line pattern. This image reveals similar pattern as observed from SEM, Fig. 4(a).

Fig. 6 shows a close-up of the line patterns over 2 μm × 3 μm area. A graphical analysis across the cursor (yellow line in Fig. 6) is shown in Fig. 7 where a grey scale value was assigned for white = 0 and black = 256. This graph may be used to quantify the line widths by calculating the full width at half maximum (FWHM) of a given line. As shown in Fig. 8, a closer view of Fig. 6 is displayed over 1 μm × 1 μm area is displayed, while Fig. 9 exhibits a graphical analysis of a few lines in Fig. 8 along the cursor (yellow line). The line width at the FWHM was found to be 15 nm ± x, where x is the standard deviation that could be quantified by reading the widths of multiple lines from Fig. 8, or equivalently, from Fig. 6 for a higher number of lines.

0894-6507 (c) 2018 IEEE. Personal use is permitted, but republication/redistribution requires IEEE permission. See http://www.ieee.org/publications_standards/publications/rights/index.html for more information.

This article has been accepted for publication in a future issue of this journal, but has not been fully edited. Content may change prior to final publication. Citation information: DOI 10.1109/TSM.2018.2865167, IEEE Transactions on Semiconductor Manufacturing

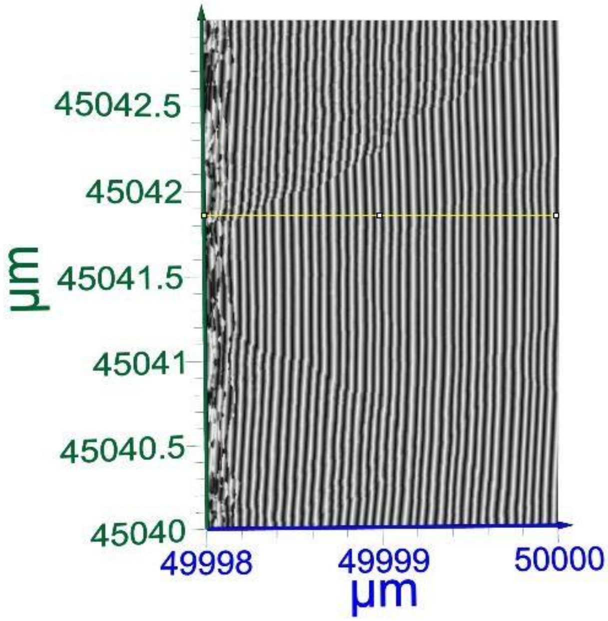

Fig. 6. Close up of line pattern extracted from Fig. 5 over 2 µm × 3 µm. The wiggly lines indicate the grain boundaries.

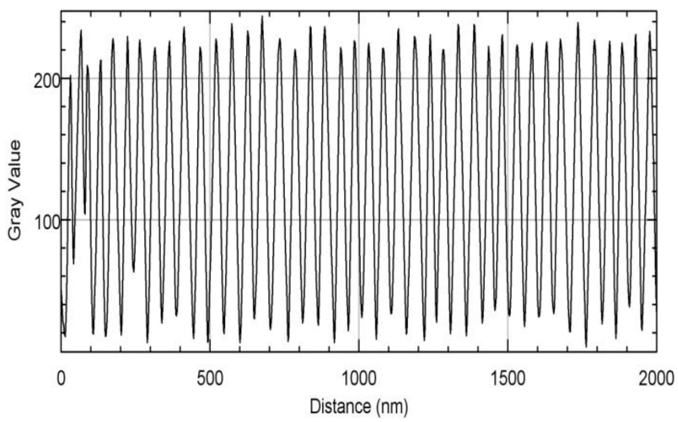

Fig. 7. Graphical analysis of the lines shown in Fig. 6. Individual line's thickness may be quantified. The yellow line in Fig. 6 may be translated at any position over the image for measuring the feature sizes at that location.

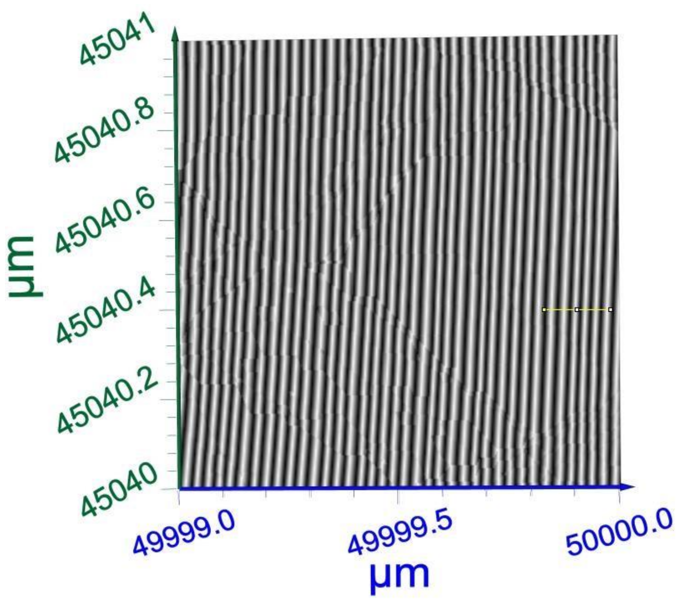

Fig. 8. A closer view of Fig. 6 over 1 µm × 1 µm shows defects in line pattern.

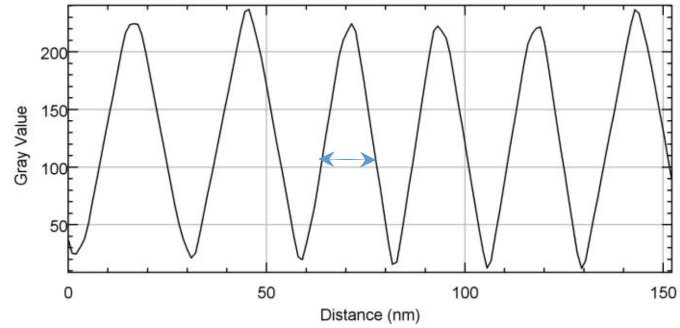

Fig. 9. Graphical analysis of Fig. 8. Calculated line width at the FWHM is ~15 ± x nm.

Fig. 10 displays a 3D view of a segment of the second sample with 70 nm line pattern and a grey-scale surface image of the same is shown in Fig. 11. Many defects are visible. A close-up of Fig. 11 is shown in Fig. 12, and Fig. 13 shows a graphical analysis of the same. The line width at FWHM was found to be 70 nm ± x nm, where x is the standard deviation that could be quantified by reading the widths of multiple lines from Fig. 11 or Fig. 12.

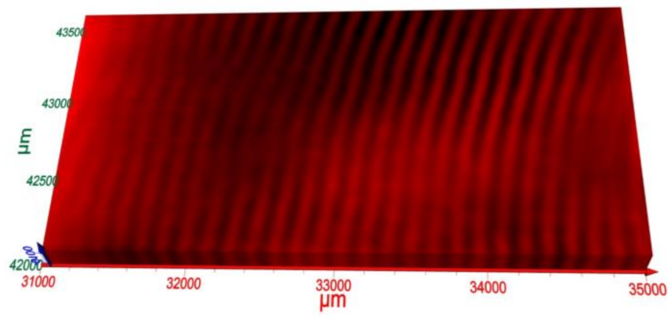

Fig. 10. Terahertz image 3-D rendering of 70 nm lines.

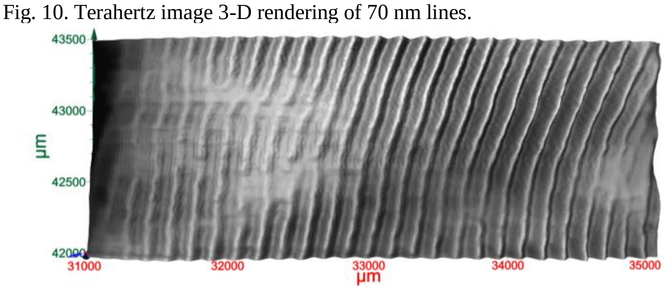

Fig. 11. Defects visible in 70 nm line pattern. Lines are curved presumably due to lack of proper alignment of the sample with respect to the beam.

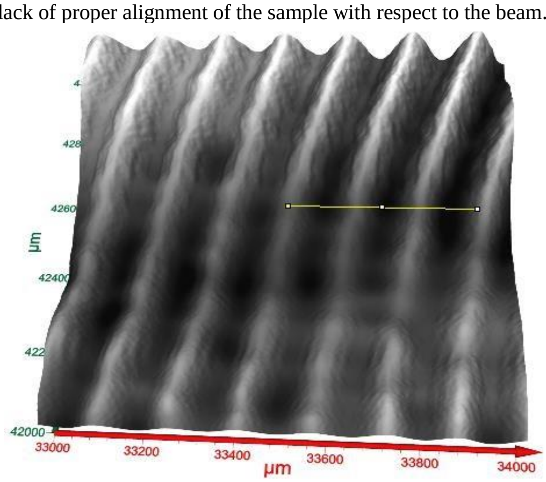

Fig. 12. Close up surface image of a few lines extracted from Fig. 11.

0894-6507 (c) 2018 IEEE. Personal use is permitted, but republication/redistribution requires IEEE permission. See http://www.ieee.org/publications_standards/publications/rights/index.html for more information.

This article has been accepted for publication in a future issue of this journal, but has not been fully edited. Content may change prior to final publication. Citation information: DOI 10.1109/TSM.2018.2865167, IEEE Transactions on Semiconductor Manufacturing

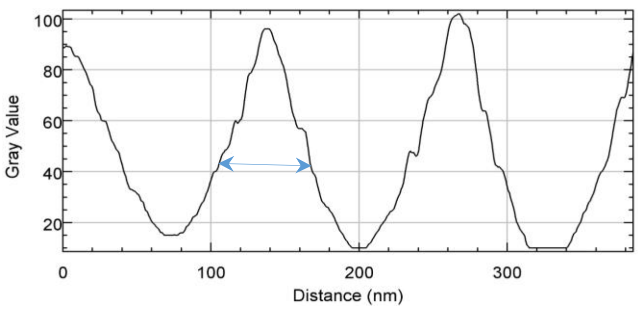

Fig. 13. Graphical analysis of Fig. 12 along the cursor. The patterned lines are ~ (70 ± x) nm.

A. *Layer by layer inspection and grain-image*

Fig. 14 shows a 3D view of 1 μm^3 volume of the first chip containing 14 nm lines from which 3 different layers on the XY plane have been extracted (Fig. 15(a)). As can be seen, the grain pattern is different on different layers. A single layer from Fig. 15(a) is shown in Fig. 16(a) whose graphical analysis is shown in Fig. 17(a) along the cursor (yellow line in Fig. 16(a)). Grain sizes may be quantified, and the size distribution may also be computed from Fig. 17(a). Other layers on the XY plane may be analyzed in a similar fashion. In addition, layers may be extracted and analyzed on other orthogonal planes, XZ or YZ (Fig. 15(b)). Fig. 16(b) shows a surface image of a graphene sample (not discussed in this paper) used only to demonstrate sub-nanometer resolution capability. Fig 17(b) displays a graphical analysis of a small feature from Fig. 16(b) whose size was determined to be ~0.77 nm; thus, demonstrating sub-nanometer resolution.

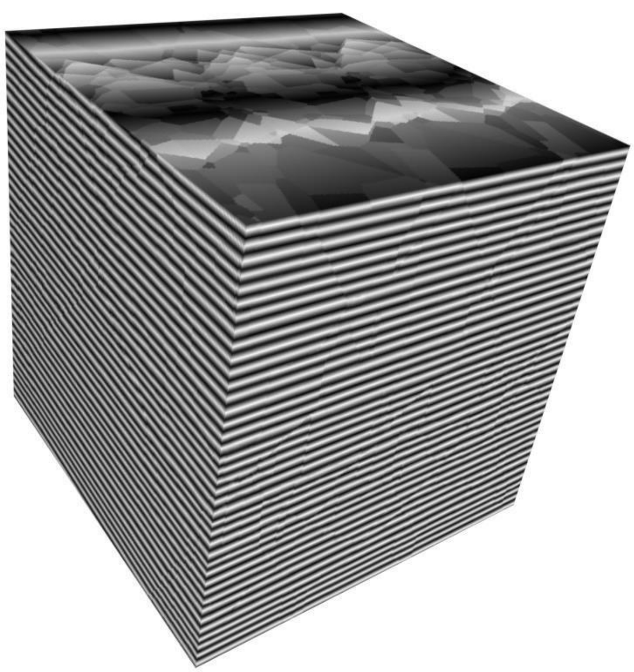

Fig. 14. 3D view of metal lines and their grain structure. 3D view of metal lines and spacings on a chip. Total volume is 1 μm^3.

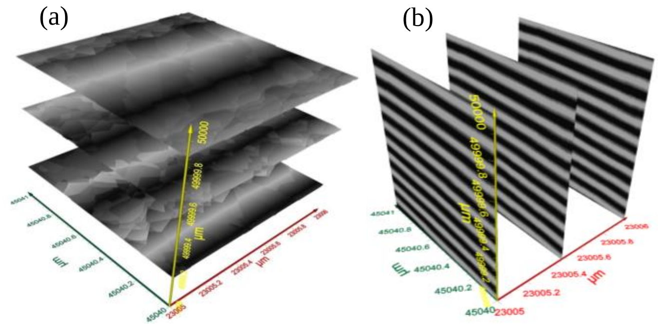

Fig. 15. (a) Layer by layer view of the grain-structure across the depth of the metal lines on the XY plane. (b) Three layers on the YZ plane.

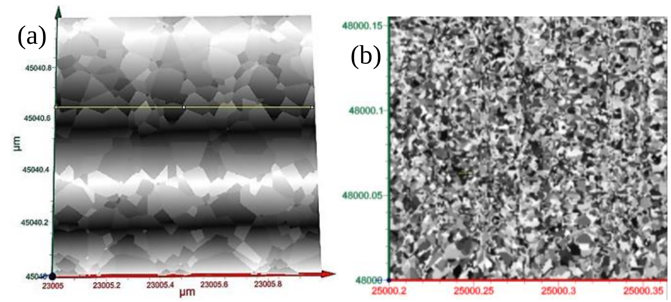

Fig. 16. (a) A single layer's (1 μm × 1 μm) grain structure on metal lines. (b) Surface image of a graphene sample (not discussed here) is used only for the demonstration of <1 nm resolution (see below).

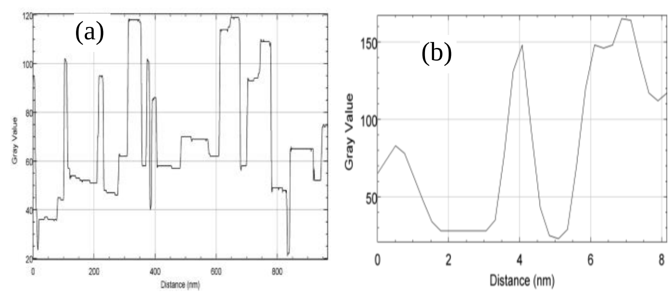

Fig. 17. (a) Analysis of grain sizes along the yellow line of the image above. The yellow line in Fig. 16 (a) may be translated at any position over the image for measuring the feature sizes at that location. (b) The FWHM is ~0.77 nm (from Fig. 16 (b)).

V. CONCLUSION

We have demonstrated terahertz multispectral reconstructive imaging of nanometer sized metal lines fabricated on a silicon wafer; thereby demonstrating that the Abbe diffraction limit has been overcome for higher resolution imaging. It was further demonstrated that while overcoming the Abbe diffraction limit is a required condition, it is not sufficient for achieving sub-nanometer resolution. A stratagem was implemented via a nanoscanner, and reflectance measurements were conducted by exploiting the Beer-Lambert law written in terms of the reflectance. A continuous wave terahertz system was used in conjunction with the said 3D nanoscanner for scanning a small volume of the samples under investigation. The "inverse distance to power equations" was used for both 2D and 3D image formation and analysis. The terahertz images were further analyzed by a graphical technique for computing the line widths from the FWHM. It was found that the line widths obtained from terahertz images are in good agreement with the

0894-6507 (c) 2018 IEEE. Personal use is permitted, but republication/redistribution requires IEEE permission. See http://www.ieee.org/publications_standards/publications/rights/index.html for more information.

This article has been accepted for publication in a future issue of this journal, but has not been fully edited. Content may change prior to final publication. Citation information: DOI 10.1109/TSM.2018.2865167, IEEE Transactions on Semiconductor Manufacturing

corresponding SEM images. Additionally, layer by layer analysis was demonstrated by dividing the terahertz images into a number of slices. Grains are clearly visible on the metal lines; their sizes may be quantified by the same graphical means as used for the line widths. Unlike electron microscope techniques where the samples must be cut to fit in the vacuum chamber and must be thin enough for electron beam transparency, terahertz imaging is a non-destructive, non-contact technique without any laborious sample preparation. There are no restrictions on the sample size or shape. The technique described herein, therefore, may be used for analysis of semiconductor features in a non-destructive, non-contact mode during the process development and at the post-process stages after device fabrication. The system can be used either in a laboratory setting or in a cleanroom environment. In addition, nanoparticles' size and size distribution may also be measured by this technique.

VI. Acknowledgement

Anis Rahman wishes to acknowledge help from Mr. Michael Hoffman of Designlynx Technology for obtaining the samples from NGR Inc.

VII. References

[1] E. Abbe, "Beiträge zur Theorie des Mikroskops und der mikroskopischen Wahrnehmung," *Arch. Mikrosk. Anat.* Vol. 9, pp. 413, 1873.

[2] L. Novotny and B. Hecht, "Propagation and focusing of optical fields," in *Principles of Nano-Optics*, Cambridge U Press, 2006, pp. 45–87.

[3] A. Rahman, A. K. Rahman, T. Yamamoto, and H. Kitagawa, "Terahertz sub-nanometer sub-surface imaging of 2D materials." *J. Biosens. Bioelectron*., vol. 7, no. 3, pp. 1–8, 2016, DOI: 10.4172/2155-6210.1000221.

[4] A. Rahman, and A. K. Rahman, "Terahertz spectroscopic analysis and multispectral imaging of epitaxially grown semiconductors with nanometer resolution," *J. Biosens. Bioelectron*., vol. 7, no. 4, pp. 1–6, 2016, DOI: 10.4172/2155-6210.1000229.

[5] A. Rahman, A. K. Rahman, and B. Rao, "Early detection of skin cancer via terahertz spectral profiling and 3-D imaging." *Biosens. Bioelectron.*, vol. 82, pp. 64–70, Aug. 2016.

[6] J. C. Davis, "*Statistics and Data Analysis in Geology*," John Wiley and Sons, NY: New York, 1986, pp. 238–244.

[7] R. Franke, "Scattered data interpolation: test of some methods," *Mathematics of Computations*, vol. 33, pp. 181-200, 1982.

[8] M. Hoffman, private communication, Oct. 2016. Although no scales are shown on the SEM images of Fig. 4, the dimensions of each feature are clearly noted in the NGR Inc. source file.

[9] A. Rahman, A. Rahman, and D. Tomalia, "Dendrimer dipole excitation: a new mechanism for terahertz generation," *J. Biosens Bioelectron*, pp 1–6, 2016, 7:196, DOI:10.4172/2155-6210.1000196

[10] A. Rahman, A. K. Rahman, and D. A. Tomalia, "Engineering dendrimers to produce dendrimer dipole excitation based terahertz radiation sources suitable for spectrometry, molecular and biomedical imaging," *Nanoscale Horizons*, vol. 2, March 20, pp. 127–134, 2017, DOI: 10.1039/c7nh00010c.

[11] A. Rahman, "Terahertz multispectral imaging of epitaxially grown semiconductors' lattice defects," *ASMC*, 2017, pp. 45–50.

Anis Rahman was born in the village of Nowbaria, Pabna, Bangladesh. He received B.Sc. (honors) and M. Sc. (first class) in physics from the University of Rajshahi, Bangladesh. From 1981 to 1985, he was a scientific officer of Bangladesh Atomic Energy Commission. He pursued an M.S. at Marquette University. He also earned Ph.D. degree in electrical and computer engineering in 1994 from the same university. He then pursued a postdoctoral research position at Columbia University under Prof. Nicholas Turro and Prof. Chris Durning.

Dr. Rahman is an acclaimed scientist in the field of nanotechnology. He is a winner of many scientific awards including NASA Nanotech Brief's "Nano-50" award twice; CLEO/Laser Focus World's "Innovation award;" and "2015 MP Corrosion Innovation of the Year," by the NACE.

Anis is the founder of Applied Research & Photonics (ARP) a leading terahertz company located in Harrisburg, Pennsylvania (see http://arphotonics.net). His invention of "Dendrimer Dipole Excitation," a new mechanism for terahertz generation, makes it possible to generate high power terahertz radiation. Anis is a recognized scientific leader and member of professional organizations including the American Chemical Society (ACS), The Optical Society of America (senior member), and the SPIE. In 2017 Anis was elected the Chair of OSA's metrology technical group. He is the past chair of the Small Chemical Businesses Division of the ACS (www.acs-schb.org). He also received awards from other scientific organizations such as the OMICS International keynote recognition; Center for Dermal Research of Rutgers University; Center for Entrepreneurial Leadership award by the Juniata College of Pennsylvania; and community awards.

Aunik K. Rahman was born in Dhaka, Bangladesh. He received B.S. in electrical engineering from Rensselaer Polytechnic Institute in Troy, NY, in 2006. Since then he has been with Applied Research & Photonics as an engineer.

Aunik's experience includes design and implementation of terahertz instruments for reconstructive imaging and time-domain spectroscopy. Aunik has received achievement awards for his work at ARP.

0894-6507 (c) 2018 IEEE. Personal use is permitted, but republication/redistribution requires IEEE permission. See http://www.ieee.org/publications_standards/publications/rights/index.html for more information.